Thermal Response on the Microstructure and Texture of ECAP and Cold-Rolled Pure Magnesium

SOMJEET BISWAS, D. SATYAVEER SINGH, BENOÎT BEAUSIR, LASZLO S. TOTH, and SATYAM SUWAS

This paper deals with dynamic recrystallization (DRX), static recrystallization, and grain growth phenomena of pure magnesium after equal channel angular pressing (ECAP) by route A and B_C at 523 K (250 °C) followed by 80 pct cold rolling. The ECAP-deformed and the subsequently rolled samples were annealed at 373 K and 773 K (100 °C and 500 °C). The associated changes in the microstructure and texture were studied using electron back-scattered diffraction. ECAP produced an average grain size of ~12 to 18 μm with B and C_2 fiber textures. Subsequent rolling led to an average grain size ~8 to 10 μm with basal texture fiber parallel to ND. There was no noticeable increase in the average grain size on annealing at 373 K (100 °C). However, significant increase in the average grain size occurred at 773 K (500 °C). The occurrence of different DRX mechanisms was detected: discontinuous dynamic recrystallization was attributed to basal slip activity and continuous dynamic recovery and recrystallization to prismatic/pyramidal slip systems. Only continuous static recrystallization could be observed on annealing.

DOI: 10.1007/s11661-015-2846-z

I. INTRODUCTION

THE interest in deformation processing of magnesium and its alloys has spurted due to its possible application in automobile, aerospace, and electronics industries, owing to the light weight (1.7 g/cm^3), superior specific stiffness, and specific strength.[1] However, the application potential is impeded by poor formability and limited ductility at room temperature, which is attributed to the limited number of operating slip systems due to the hexagonal crystal structure of magnesium.[2,3] Equal channel angular pressing (ECAP) has been proved to be very effective in enhancing the workability as well as the strength of Mg alloys by enabling rolling[4] and ECAP[5] at room temperature. The enhanced ductility is attributed to an initial grain refinement,[4–10] characteristic shear texture[11–14] due to ECAP, and the consequence of anisotropic stacking fault energy in pure magnesium.[5] An important aspect of severe plastic deformation, particularly at lower temperatures, is the accumulation of a large amount of stored energy, which in generally leads to kinetically driven microstructural changes in a course of time. It is therefore desirable to reduce the stored energy by a post-deformation recovery and static recrystallization (SRX) process[15,16] to obtain stable microstructure for application purposes. This becomes particularly relevant for the case of magnesium, where the activation energy barrier for such thermally activated processes is quite low.

It is well known that high-temperature deformation of Mg leads to bimodal grain size distribution due to dynamic recrystallization (DRX).[17–20] It is usually believed that on annealing the grain size distribution changes into a singular peak.[20–22] As the annealing temperature increases, the grains become larger, however, no appreciable change in the texture occurs.[23,24] Several authors have reported that the inclination of basal pole toward the normal direction (ND) of a sheet reduces on annealing.[25–27] Huang *et al.*[28] have shown that rolling at high temperatures eliminates the basal pole inclination to ND due to DRX. Low-temperature rolling suppresses DRX and post-deformation annealing retains the deformation texture inclination that is favorable for further workability. Although DRX occurs during plastic deformation, a large fraction of dislocations could be present. These dislocations could be reduced by SRX. There are several studies[29–31] on annealing behavior of Mg alloys. Lu *et al.*[32] show that SRX grains formed *via* extension twinning maintain their orientation. On the other hand, Ostapovets *et al.*[33] have found that the 30 deg misorientation characteristic among DRX grains is attributed to Σ13a or Σ15a

SOMJEET BISWAS, Assistant Professor, is with the Department of Metallurgical and Materials Engineering, Indian Institute of Technology Kharagpur, Kharagpur 721302, India, also with the Department of Materials Engineering, Indian Institute of Science, Bangalore 560012, India, and also with the Laboratory of Excellence on Design of Alloy Metals for low-mAss Structures (DAMAS), Université de Lorraine, 57045 Metz, France. Contact e-mail: somjeetbiswas@gmail.com D. SATYAVEER SINGH, Project Assistant, is with the Department of Materials Engineering, Indian Institute of Science. BENOÎT BEAUSIR, Assistant Professor, and LASZLO S. TOTH, Professor, are with the Laboratory of Excellence on Design of Alloy Metals for low-mAss Structures (DAMAS), Université de Lorraine, and also with the Laboratoire d'Étude des Microstructures et de Mécanique des Matériaux, UMR 7239, CNRS/Université de Lorraine, 57045 Metz, France. SATYAM SUWAS, Associate Professor, is with the Department of Materials Engineering, Indian Institute of Science.

Manuscript submitted March 10, 2014.
Article published online March 20, 2015

coincident site lattice relationship. A clear understanding of the underlying physical process that controls the microstructure and texture evolution during recrystallization of Magnesium has not yet been developed due to the complexity of the process.

In the present article, a detailed analysis of the microstructure and texture of pure magnesium has been carried out after 523 K (250 °C) ECAP by route A and B_C and subsequent room temperature rolling followed by annealing. The mechanisms related to dynamic and SRX as well as grain growth are examined. The annealing of the deformed specimens was carried out at two extreme temperatures: at 373 K (100 °C) to examine the thermal stability, and at 773 K (500 °C) to examine the high-temperature response of the microstructure and the texture.

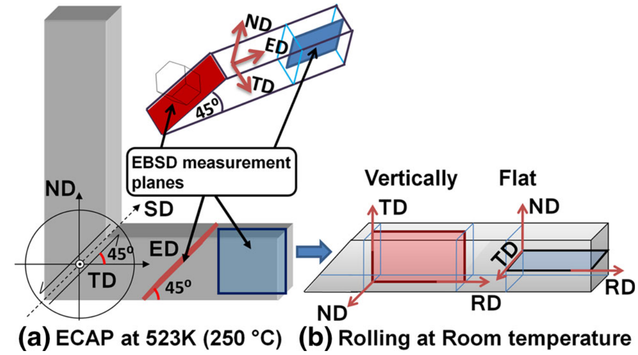

Fig. 1—Schematic depiction of (*a*) the ECAP process and (*b*) the subsequent rolling scheme. The planes on which the EBSD scans were obtained, as well as the reference frame for the pole figure representation are shown.

II. EXPERIMENTAL METHODS

A. *Processing*

Hot forged magnesium with 99.9 pct purity was processed by ECAP up to four passes at 523 K (250 °C) following routes A and B_C. ECAP route A corresponds to no rotation around the billet's longitudinal axis and route B_C to an anti-clockwise rotation by 90 deg between passes.[4,5] Figure 1(a) shows the sample coordinate system for ECAP; ED is the ECAP direction, ND is the normal direction, and TD is the transverse direction. The ECAP samples were prepared keeping ND parallel to the forging direction. An optimally designed die with a channel angle of 90 deg was used.[34] The dimensions of the Mg billets were 10 mm × 10 mm × 100 mm. Subsequently, room temperature rolling was performed on the ECAP route B_C-processed samples up to 80 pct thickness reduction. Two initial sample orientations were chosen for rolling. In the first case, the samples were rolled so that the ND of rolling was parallel to the transverse direction (TD) of the ECAP-processed sample, and is termed as vertically rolled (VR) case. In the second case, the ND of the rolled samples was parallel to the ND of the ECAP-processed sample and is named flat-rolled (FR) case. This is explained schematically in Figure 1(b). The rolling direction is abbreviated as RD. Isothermal annealing at the temperatures 373 K and 773 K (100 °C and 500 °C) under argon atmosphere was carried out for 1 hour for the only ECAP-deformed as well as the VR and FR samples.

B. *Characterization*

Samples from the only ECAP-processed billet were cut on two planes: parallel to the TD plane of the ECAP reference system (TD-cut) as well as on the plane 45 deg with respect to the ED and ND directions of the billet (shear plane cut), see Figure 1(a). For all rolled and annealed samples, the microstructure was examined on the rolling (ND) plane. The texture measurements and microstructural characterizations were carried out using the electron back-scatter diffraction (EBSD) technique in a scanning electron microscope (FEG-SEM) equipped with a field emission gun. The samples for EBSD were prepared by conventional metallurgical technique followed by chemical polishing using a solution of 75 pct ethanediol, 24 pct distilled water, and 1 pct HNO_3 to obtain a mirror finish. At the end, electro-polishing was performed in ethanol and orthophosphoric acid in a ratio of 3:5, using a stainless steel cathode at 3 V for 30 second and 1.5 V for 2 minutes at ~0 °C. Partitioning of the EBSD-generated micrographs was carried out to separate the recrystallized grains from the deformed ones using image quality (IQ) criteria. Detailed texture analysis was performed using the EBSD measurements by plotting the pole figures and orientation distribution functions (ODF) in three-dimensional Euler space.

III. RESULTS

A. *Microstructure*

The starting material had a granular microstructure with an average grain size of ~200 μm calculated from linear intercept method using optical microscopy. X-ray goniometric study showed strong basal poles parallel to the forging direction.

B. *Microstructures Obtained by ECAP and by Subsequent Annealing*

1. *After ECAP only*

The inverse pole figure (IPF) maps generated by EBSD scans on the TD plane of pure Mg after four ECAP passes by routes A and B_C and after subsequent annealing at 373 K (100 °C) and at 773 K (500 °C) for 1 hour are shown in Figure 2. For the as-ECAP samples, most of the grains are equiaxed with serrated grain boundaries, and a few slightly elongated larger grains are present. The grain size distributions for both the ECAP routes and after subsequent annealing are shown in Figure 3. The number fraction average grain sizes are ~6.2 and ~5.9 μm for ECAP routes A and B_C, respectively.

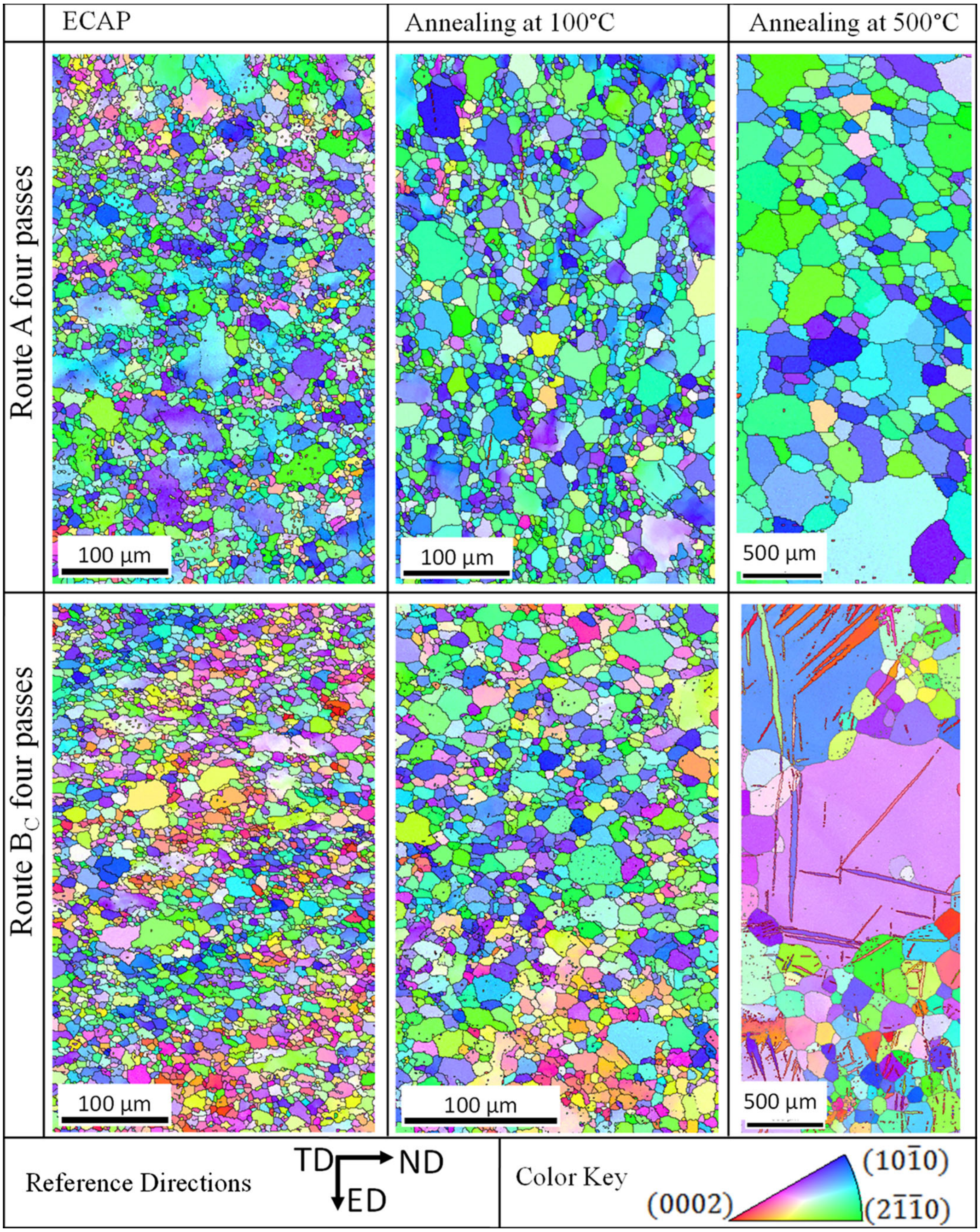

Fig. 2—Inverse pole figure (IPF) maps of the Route A and B_C ECAP-processed pure Mg after four passes, and after subsequent annealing at 373 K and 773 K (100 °C and 500 °C).

The number fraction method is the usual method of obtaining average grain sizes in most literatures related to ultra-fine grains and nano-technology. However, in cases which involve large grain size ranges and diverse grain size distributions (Figure 3), it is more appropriate to examine the grain size distribution by the *area fraction* method. This is due to the fact that the contribution of the larger grains on any physical property of the material is more. The average grain size calculated by the number fraction method usually has a smaller value than by the area fraction method.[35,36] Using this method, the obtained average grain sizes were ~17 and ~12 μm, for the ECAP routes A and B_C, respectively. All average grain sizes shown further in this paper are calculated using the area fraction method.

2. *After annealing*

The stability of the microstructure was analyzed by annealing the samples after ECAP at 373 K (100 °C) and at 773 K (500 °C) for 1 hour. A small increase in the grain size to ~19 and 13 μm was observed at 373 K (100 °C) for both routes (Figure 2). On the other hand, annealing at 773 K (500 °C) led to an increase in the grain size to ~270 μm for both routes (Figure 2). The

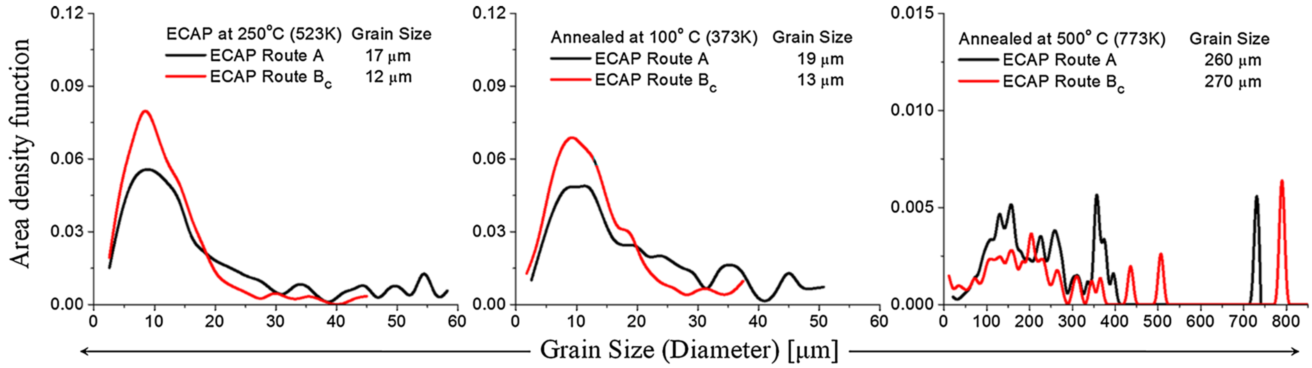

Fig. 3—Grain size distribution plots of the route A and B_C ECAP-processed pure Mg after four passes, and after subsequent annealing at 373 K and 773 K (100 °C and 500 °C).

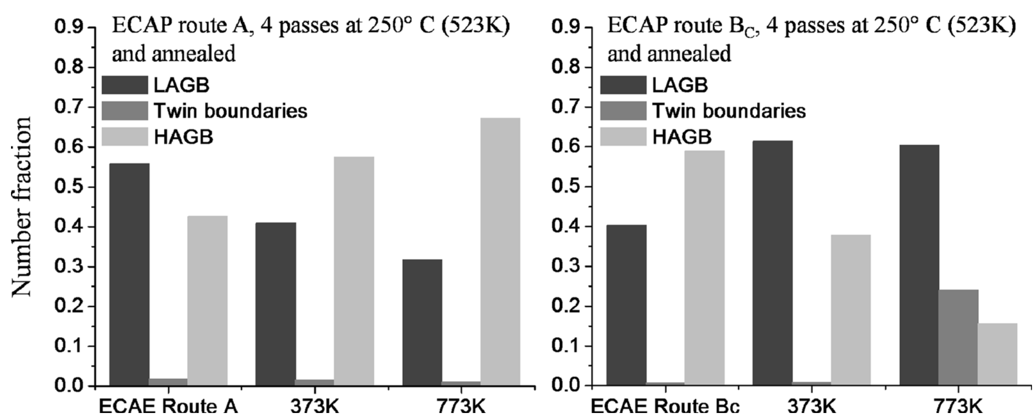

Fig. 4—Grain boundary character distribution (GBCD) in pure Mg obtained in ECAP routes A and B_C after four passes as well as after subsequent annealing at 373 K and 773 K (100 °C and 500 °C).

grain size distribution after annealing at 373 K (100 °C) as well as at 773 K (500 °C) is shown in Figure 3.

The grain boundary character distribution (GBCD) was analyzed with the help of the misorientation angle distribution obtained from the EBSD scans. We have chosen three characteristics for GBCD: the low-angle grain boundaries (LAGB), the high-angle grain boundaries (HAGB), and the $\{10\bar{1}2\}$ extension twin boundaries (Figure 4). Contraction or double twins could not be detected.

C. *Microstructures Obtained by ECAP + Cold Rolling and Annealing*

After four ECAP passes by route B_C, the magnesium samples were rolled at room temperature in the VR and the FR configuration. The IPF maps shown in Figure 5 were captured on the ND plane. The corresponding annealed micrographs are also presented in this figure. For both conditions (VR or FR), an average grain size of ~8 to 10 μm was obtained after 80 pct rolling. The presence of elongated grains and surrounding smaller equiaxed grains can be noted. The grain size distributions are displayed in Figure 6 for all cases. The microstructural features indicate the occurrence of DRX, though to a lesser extent than in the only ECAP-processed samples.

The grain size range remained almost the same after annealing at 373 K (100 °C) for 1 hour but increased largely after the 773 K (500 °C) treatment (Figures 5, 6). On annealing at 373 K (100 °C), the average grain size was ~10 to 11 μm for both VR and FR samples. However, after annealing at 773 K (500 °C), the average grain size increased to ~250 μm. The GBCD plots obtained from the EBSD scans after rolling (VR and FR) and annealing are presented in Figure 7. A smaller amount of DRX took place in the room temperature rolling cases compared to the only ECAP-processed samples, thus, comparatively a larger LAGB fraction was observed (compare Figures 4, 7).

IV. TEXTURE

A. *After ECAP and Subsequent Annealing*

Figure 8 shows the (0002) and $(11\bar{2}0)$ pole figures and the $\varphi_2 = 0$ deg and 30 deg sections of orientation distribution functions (ODFs) for the ECAP-processed pure Mg by routes A and B_C and the respective annealed samples. The important ideal end orientations of HCP Mg crystal in simple shear *i.e.*, the B and the C_2 fibers corresponding to basal and pyramidal $\langle c + a \rangle$ type-II slips, respectively, are marked in the figures.[37] In the case of ECAP by route A, the orientation maxima

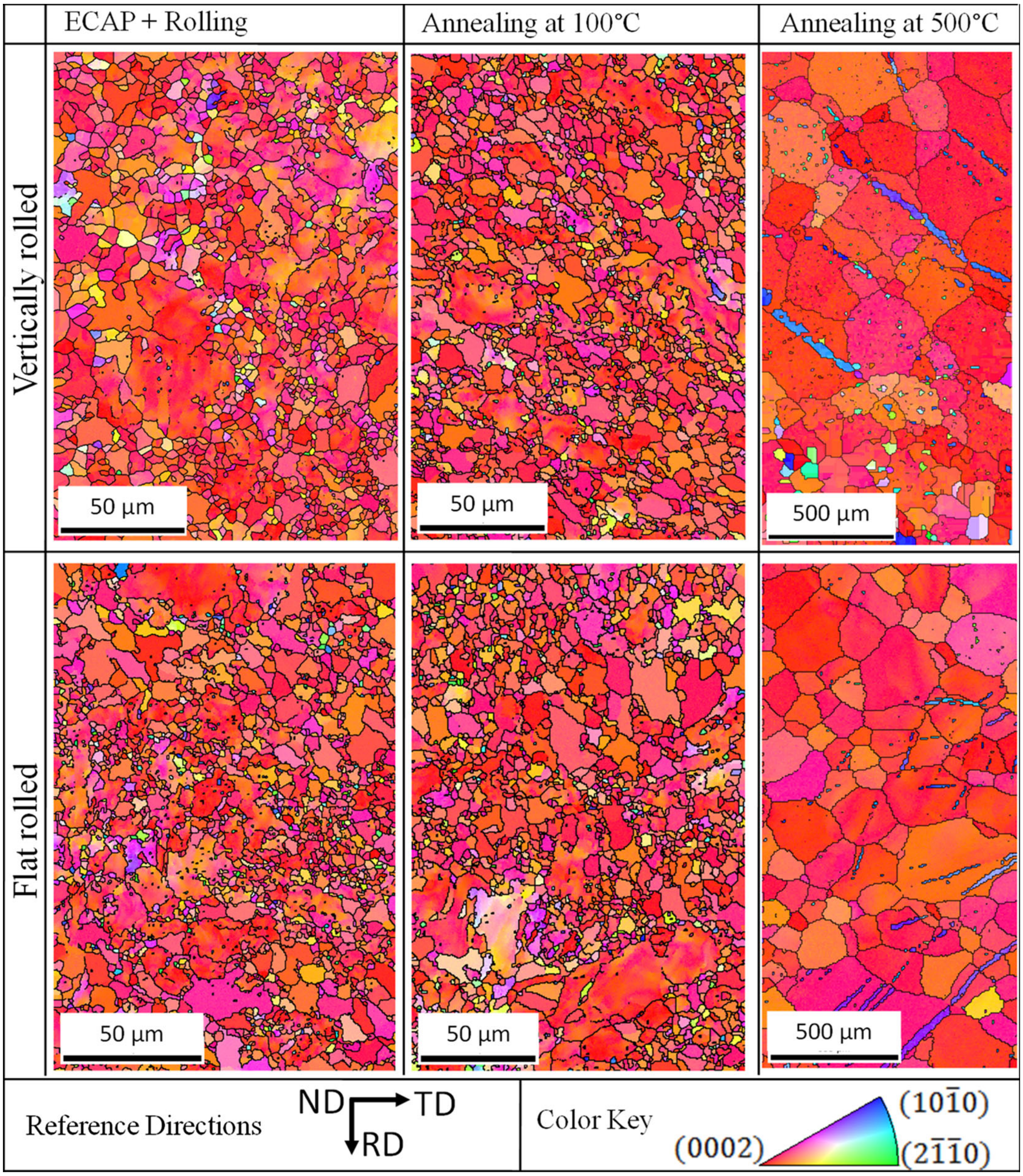

Fig. 5—Inverse pole figure (IPF) maps obtained after room temperature rolling of previously ECAP-deformed samples in vertically (VR) and flat (FR) positions as well as after subsequent annealing at 373 K and 773 K (100 °C and 500 °C). ECAP was done by route B_C up to four passes.

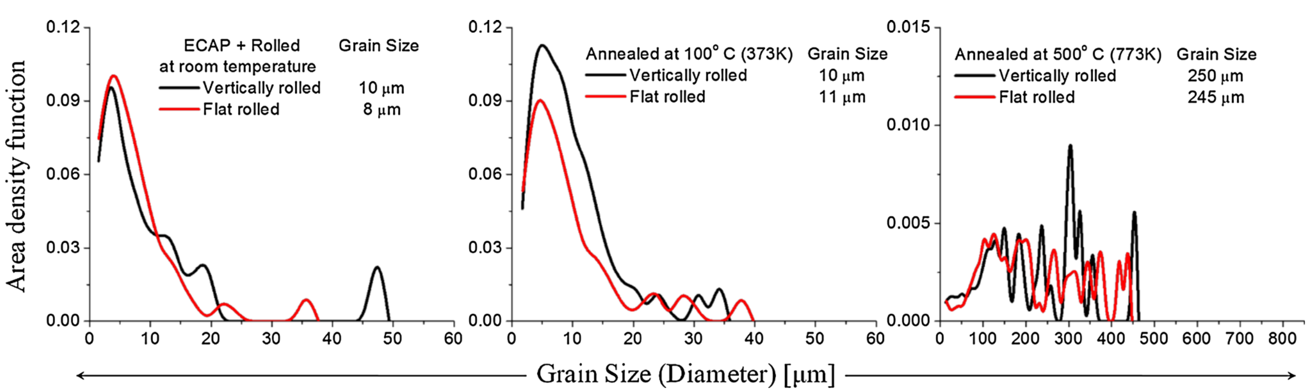

Fig. 6—Grain size distribution plots of the room temperature vertically rolled and flat-rolled (VR and FR) pure Mg, and after subsequent annealing at 373 K and 773 K (100 °C and 500 °C).

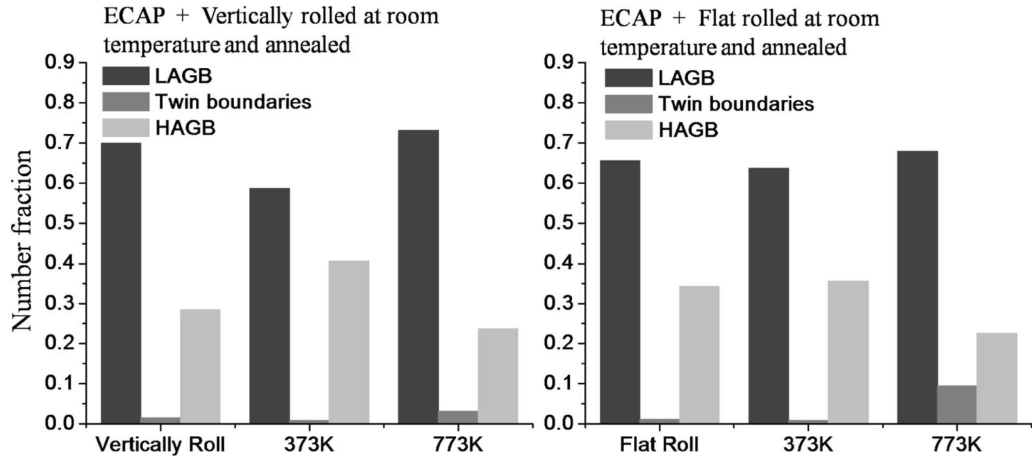

Fig. 7—Grain boundary character distribution (GBCD) obtained after room temperature rolling of previously ECAP-deformed samples in vertical (VR) and flat (FR) positions as well as after subsequent annealing at 373 K and 773 K (100 °C and 500 °C). ECAP was done by route B_C up to four passes.

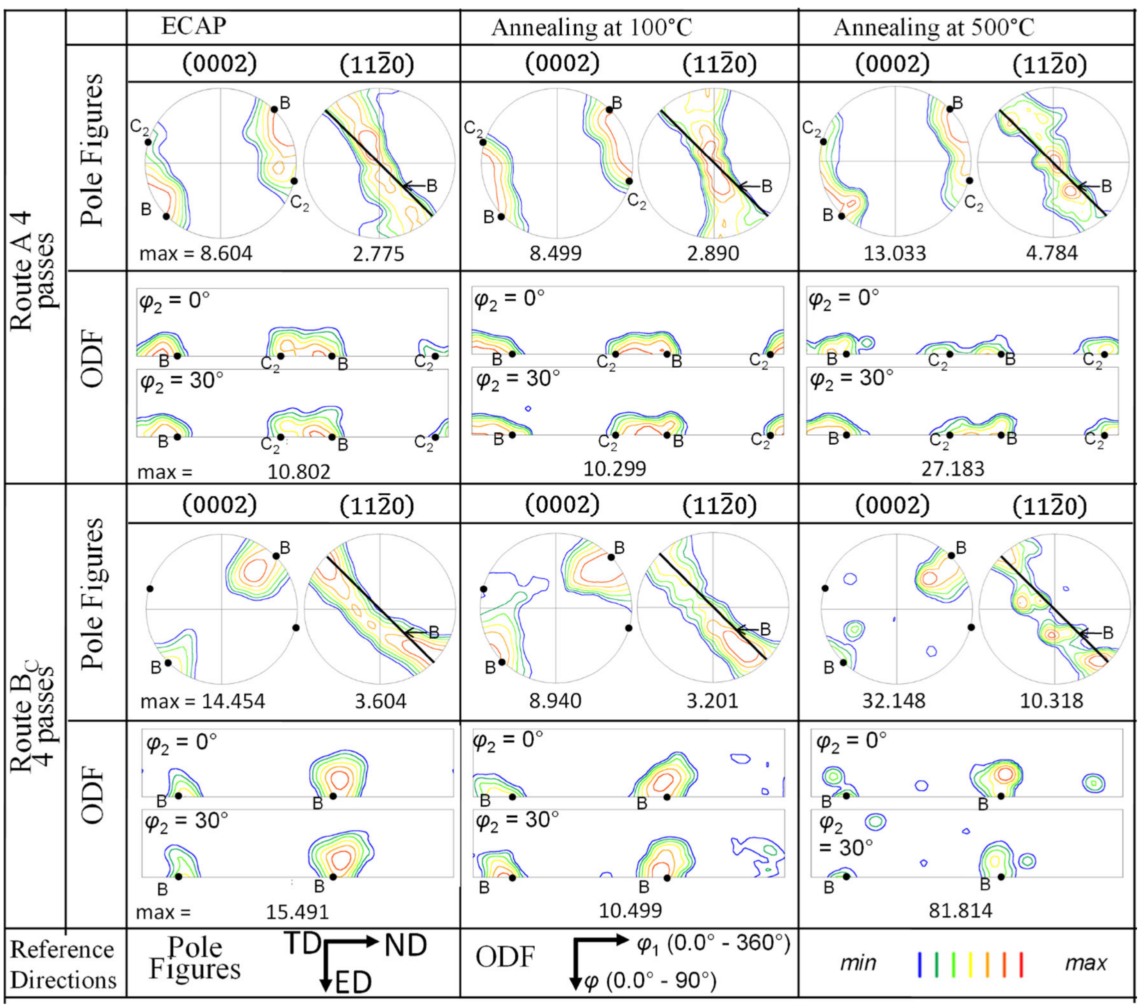

Fig. 8—(0002) and (11$\bar{2}$0) pole figures and φ_2 = 0 deg and 30 deg ODF sections of the route A and B_C ECAP-processed pure Mg after four passes, and after subsequent annealing at 373 K and 773 K (100 °C and 500 °C).

exhibited a tendency to approach the ideal B fiber position[38]; for route B_C, an asymmetric B fiber formed around ND. It has been shown previously[35,39] that the effect of dynamic recrystallization on the texture of Mg alloys can be readily observed in the φ = 90 deg ODF section. In Figure 9, the φ = 90 deg ODF section for

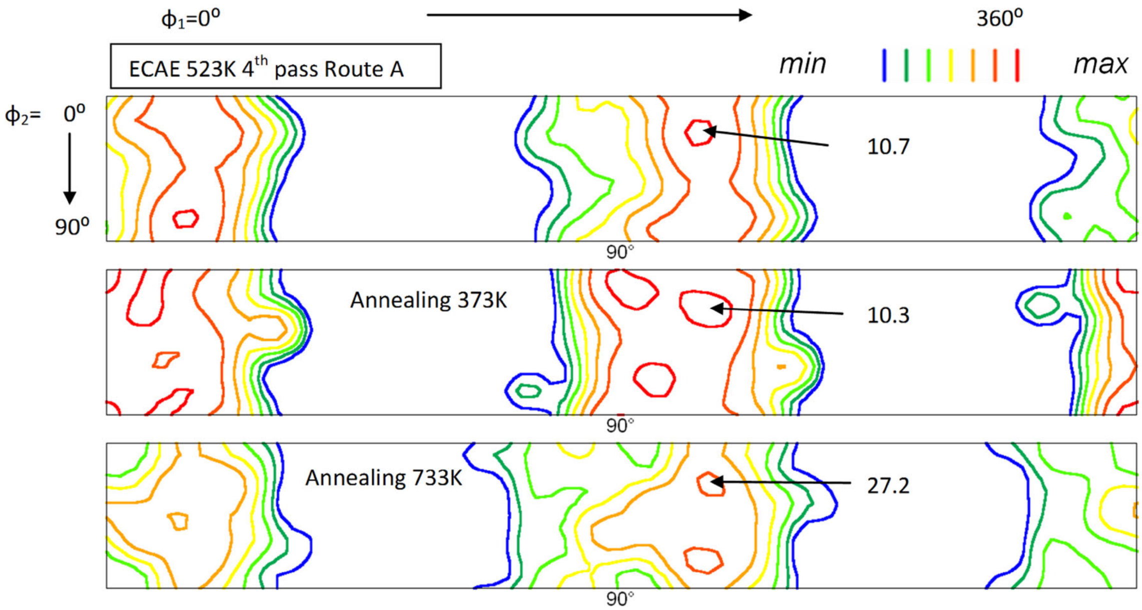

Fig. 9—φ = 90 deg ODF section of the route A ECAP-processed pure Mg after four passes, and after subsequent annealing at 373 K and 773 K (100 °C and 500 °C).

the ECAP (route A)-processed Mg is shown. The texture fiber appeared in the range φ_2 = 0 to 60 deg, with a maximum at $\varphi_2 \approx 20$ deg (black arrow). The position of maximum texture intensity ($f(g)_{max}$) on the texture fiber remained the same even after annealing, nevertheless, the value of $f(g)_{max}$ increased from ~10.8 to ~27 on annealing at 773 K (500 °C). A similar trend was observed also for route B_C. The texture maximum intensity $f(g)_{max}$ increased from ~15.4 to ~82.

B. *ECAP + Cold Rolled and Subsequent Annealing*

Figure 10 shows the (0002) and $\left(11\bar{2}0\right)$ pole figures and the φ_2 = 0 deg and 30 deg ODF sections for the room temperature VR and FR cases and for the respective annealed samples. A prominent axisymmetric basal texture formed at ND after both VR and FR processing. On static annealing at 373 K (100 °C) and even at 773 K (500 °C), the texture remained predominantly basal with an increase in the peak intensity. The maximum texture intensity was observed at $\varphi \approx 20$ deg for the rolled and annealed samples.

The IPF maps (Figure 5) show some preferential grain growth and twin formation on annealing at 773 K (500 °C). Microstructural analysis revealed that these are mostly tensile twins corresponding to ~86 deg rotation around the $\langle 11\bar{2}0\rangle$ axis. The presence of twins can be detected as a new texture component in the (0002) pole figures and in the φ_2 = 0 deg section of the ODF (Figure 10) at a location ~90 deg away from the regular rolling texture fiber.

To analyze the effect of dynamic and SRX on texture in a distinctive manner, partitioning of the EBSD microstructures was carried out to separate the recrystallized grains from the deformed ones using an image quality (IQ) criterion. A representative IQ map taken from the rolled sample is shown in Figure 11. Once separated using such a criterion, the recrystallized grains are characterized by high IQ and appear light gray, while the low-IQ deformed grains appear dark. A typical value of IQ ≈ 20 was found suitable to separate the recrystallized and deformed grains for both the rolled and the 373 K (100 °C) annealed samples. After rolling, the recrystallized fraction was ~0.52; on annealing at 373 K (100 °C) ~0.55 for both the VR and FR cases. The microstructure was fully recrystallized on annealing at 773 K (500 °C). In order to examine any change in texture during annealing of the rolled samples, the φ = 90 deg section of the ODF was plotted from the partitioned and un-partitioned data for the rolled and the 373 K and 773 K (100 °C and 500 °C) annealed samples in Figure 12. The maximum intensity of the ODF fiber was observed at φ_2 = 0 deg for the deformed grains, and at φ_2 = 30 deg for the recrystallized grains indicating a large orientation difference between the two populations of IQ values. The Kernel average misorientation (KAM) distribution plots for the full and the partitioned microstructure with IQ > 20 and IQ ≤ 20 are shown in Figure 11. The KAM distribution curve has two regions: a lower KAM region (KAM < 0.4 deg) and a relatively higher KAM region (0.4 deg < KAM < 5 deg). In the higher KAM regions, displaying a lognormal shape, the average KAM value is the same for each case but the number fraction is lower for the partitioned microstructure with IQ ≤ 20 *i.e.*, for the deformed part of the microstructure. It means that the lognormal shape of the KAM distribution plots indicate randomly distributed micro-strains.[40] On the other hand, a high value of KAM can be observed in the lower KAM region for the deformed part of the microstructure (IQ ≤ 20). This indicates strain heterogeneity in the deformed part of the microstructure. This occurs due to heterogeneous arrangement of dislocations in the partitioned deformed microstructure. (It is to clarify that we have not analyzed the type of dislocations in this paper).

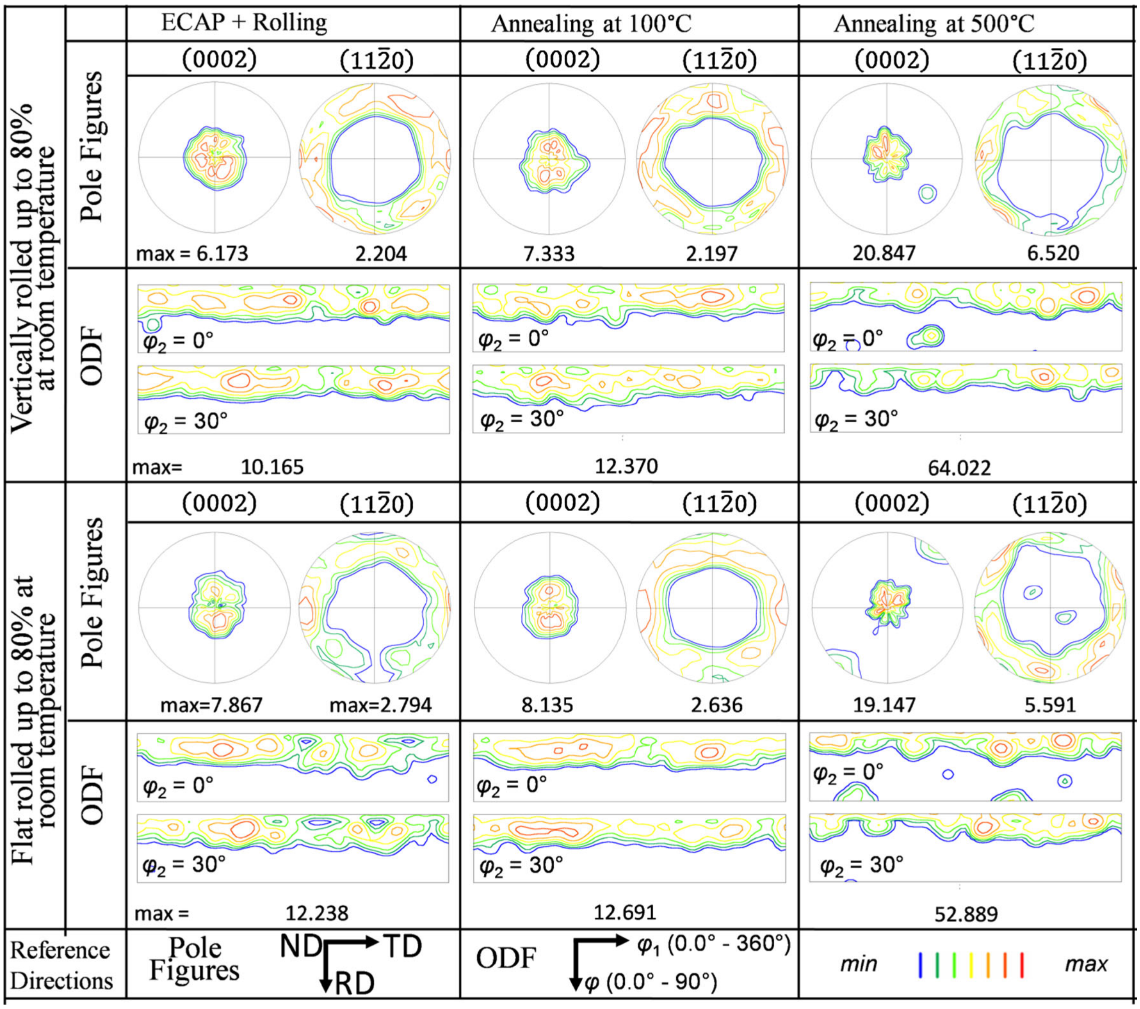

Fig. 10—(0002) and (11$\bar{2}$0) pole figures and φ_2 = 0 deg and 30 deg ODF sections of the room temperature vertically rolled and flat-rolled (VR and FR) pure Mg, and after subsequent annealing at 373 K and 773 K (100 °C and 500 °C).

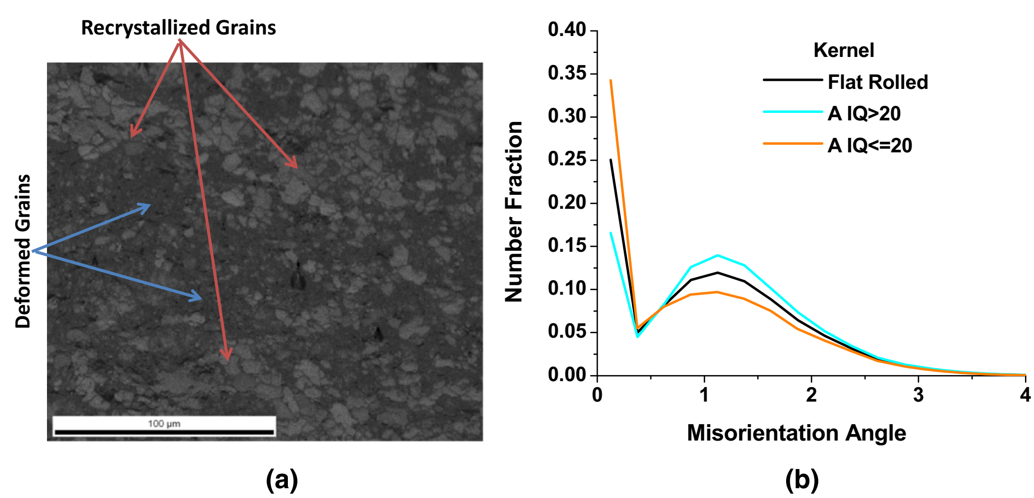

Fig. 11—(*a*) Image quality (IQ) map of the vertically rolled (VR) pure Mg and (*b*) a comparison of Kernel average misorientation (KAM) for the microstructure of the VR samples, partitioned on the basis of IQ values. Partitioning criterion: IQ > 20 for recrystallized grains, IQ ≤ 20 for deformed grains.

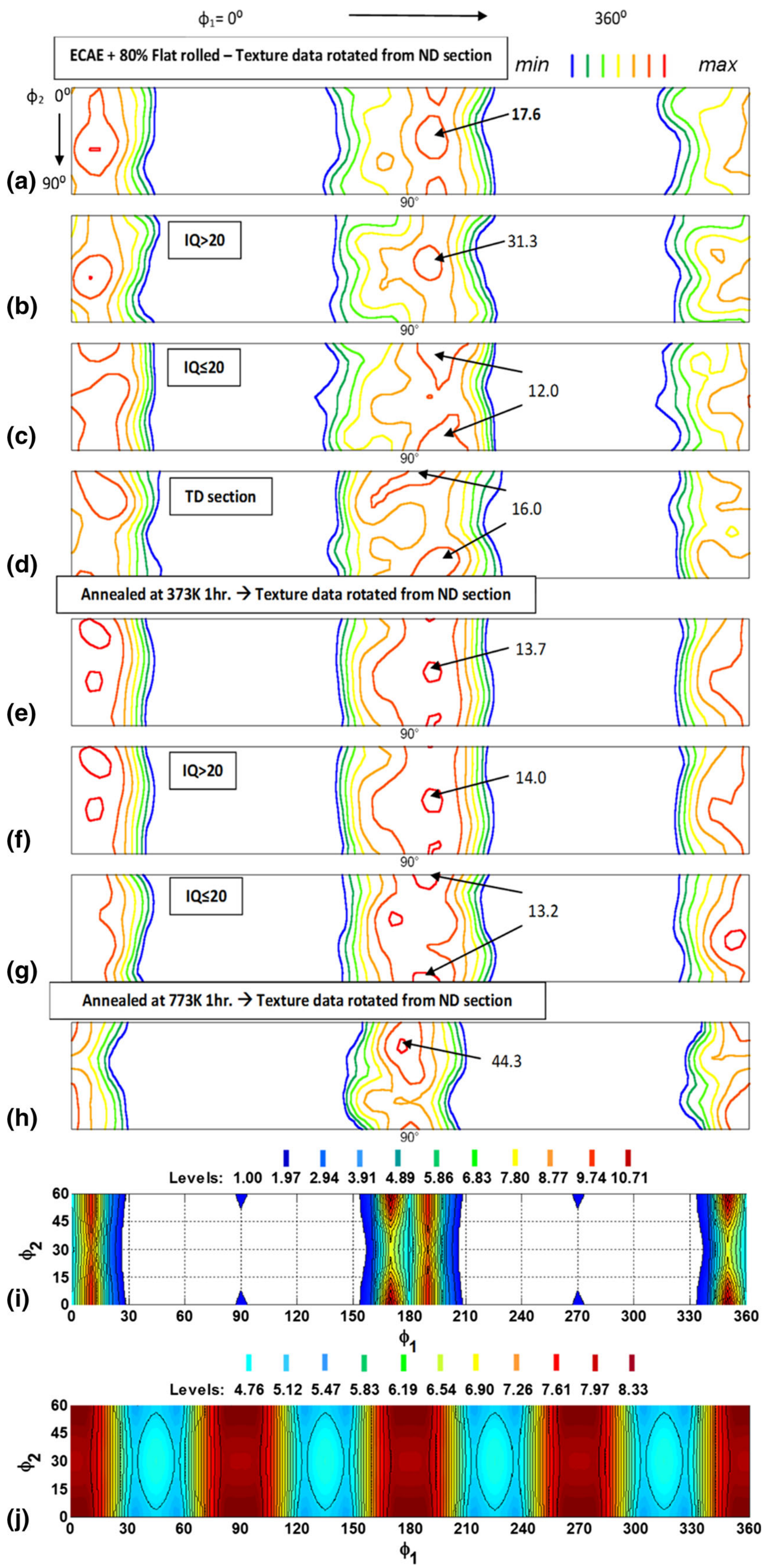

Fig. 12—φ = 90 deg ODF section of the vertically rolled (VR) pure Mg and after annealing at 373 K and 773 K (100 °C and 500 °C) and their partitioned, recrystallized, and deformed fractions. Deformation texture obtained by VPSC modeling (*i*) and the Plastic power map (*j*) is also demonstrated.

V. DISCUSSION

A. *Effect of Dynamic Recrystallization on the Microstructure*

1. *ECAP*

The strain introduced into magnesium during four ECAP passes is very high; $\varepsilon_{\text{von-Mises}}$ ~4.0, however, due to the high deformation temperature of ~523 K (250 °C), recovery and DRX could take place, and indeed it can be seen in the IPF maps (Figure 2). In order to understand the DRX mechanism in pure Mg during high-temperature severe plastic deformation, the misorientation angle boundary maps and the IPF maps of the fourth pass ECAP (route A) sample were analyzed by superimposing the HCP unit cells on the maps. The analysis was done on the TD plane (Figure 13) and on the 45 deg section along the shear plane (Figure 14). On the basis of previous investigations on ECAP of pure Mg by route A,[5,41] it is now known that the TD plane contains mostly prismatic and pyramidal planes, and the 45 deg plane contains near basal planes. The observations were made on these two planes in order to examine the orientation-dependent DRX response owing to the anisotropy in SFE of pure Mg.[42] The analysis of the TD plane (Figure 13) shows that the density of LAGBs (2 deg to 15 deg) at the vicinity of HAGBs (>15 deg) is high, and their concentration slightly decreases toward the center of the grains. Moreover, 5 deg to 15 deg misorientations (green boundaries) are also observed near the grain boundaries. This indicates a gradual increase in misorientation of the LAGBs to form HAGBs during deformation. The orientations of the deformed and the surrounding recrystallized grains were compared using superimposed hexagonal unit cells corresponding to respective grains on the magnified IPF maps (Figures 13(b) through (d)). As compared to the deformed grains, slight rotations of the unit cells around the basal axis (~30 deg from blue to green colored grains) can be observed for the recrystallized grains. This mechanism corresponds to ''continuous dynamic recovery and recrystallization'' (CDRR) corroborating previous works.[5,43,44] Ion *et al*.[45] have shown that rotational dynamic recrystallization (RDRX) occurs due to relative difficulty in operating non-basal slip systems at the temperature range of 423 K and 593 K (150 °C to 330 °C). Later, Humphrey and Hatherly[46] claimed that RDRX comes under the category of continuous dynamic recrystallization (CDRX), as in this process minimal grain boundary migration occurs and there is no clear division between the nucleation and growth stages. On the other hand, Galiev *et al*.[47] have shown that CDRX is linked with deformation controlled by cross-slip in the temperature range of ~473 K to 523 K (200 °C to 250 °C). At higher temperature, DDRX occurs due to bulging of original grain boundaries and subgrain growth controlled by dislocation climb. Tan and Tan[48] showed the occurrence of CDRX in the temperature range of 523 K to 673 K (250 °C to 400 °C) by transmission electron microscopy (TEM). Later, Biswas *et al*.[35] schematically illustrated the evolution of microstructure in magnesium during CDRR at 523 K (250 °C) in the presence of multiple slips.

The DRX mechanism pertaining to the 45 deg section of the ECAP samples can be evaluated in Figure 14. Due to the evolution of the shear texture during ECAP, the basal planes lie mostly in this 45 deg section. In this case, the orientations of the small equiaxed grains do not present a ~30 deg rotation relationship about the basal axis from the deformed grains, so the mechanism is totally different. In other words, the unit cells embedded in these recrystallized grains do not follow a gradual tilt, rather display random tilts with respect to the unit cells representing the deformed grains. Such a microstructural feature is observed during the occurrence of ''discontinuous dynamic recrystallization'' (DDRX). As an exception, at a few locations on this plane, some features of CDRR could also be observed (Figure 14(e)). A noticeable feature on this section of the sample is that the LAGBs are not concentrated near the prior grain boundaries of the deformed grains.

The fact that CDRR is mostly observed on the TD plane and DDRX on the 45 deg section is somewhat confusing. This is because DRX is not a planar process, so the DRX mechanism cannot depend on the surface of observation. In order to clarify the situation, it is important to mention that due to the deformation conditions in ECAP, the grains in the polycrystalline matrix get oriented with their basal planes parallel to the shear plane of the ECAP process in the 45 deg section. Grains oriented in this manner have prismatic/pyramidal planes aligned nearly parallel to the TD plane. Such a situation leads to anisotropic response during deformation for the following reasons: The observations on the TD plane statistically show mostly the microstructural features pertaining to the prismatic and pyramidal slip activity, and relatively less features relevant to the basal slip. As the stacking fault energies (SFE) of the prismatic and pyramidal planes are high (~265 and ~344 mJ/m^2, respectively),[42] the distance between the partials are low, and thus dislocations cross-slip lead to recovery over recrystallization during deformation. Similarly, the 45 deg sample section which contains mainly basal orientations gives a statistical coverage of the microstructural features affected by basal slip, which have low SFE (~36 mJ/m^2).[42] The wide stacking fault basal dislocation partials do not allow cross-slip and strain hardens rapidly leading to DDRX. A banded structure is usually observed (Figure 14(b)). Thus, both DRX mechanisms were active during deformation.

2. *Cold rolling*

Before discussing the DRX behavior during room temperature rolling, it is important to comment on the possibility of successful 80 pct rolling reduction at ambient temperature. This could be attributed to the microstructural features obtained after ECAP:[4] (i) the initial grain size reduction leads to an increase in toughness by reducing the propensity of cleavage fracture owing to the increased grain boundary fraction, (ii) it reduces and distributes the stress more homogeneously at the grain boundaries and triple junctions,

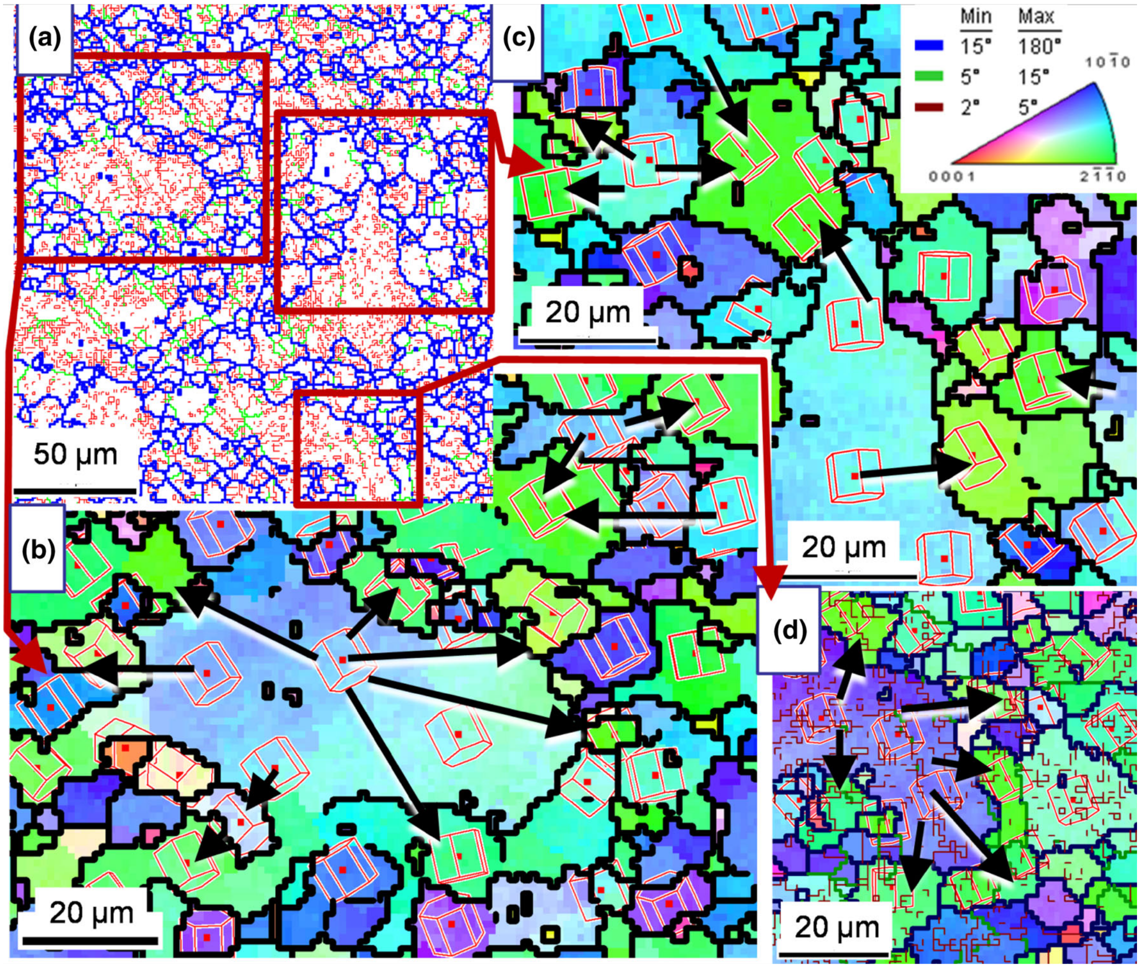

Fig. 13—Grain boundary map and magnified Inverse pole figure (IPF) maps with superimposed HCP unit cell as recorded on the TD plane of the Route A ECAP-processed pure Mg after four passes.

thus, increases the activity of prismatic/pyramidal slip and reduces the twinning activity,[38,49] (iii) the bimodal grain size distribution increases grain boundary sliding,[50] and (iv) the anisotropy in SFE leads to strain hardening of the basal slip systems and strain softening of the prismatic and pyramidal slip systems leading to a reduction of the critical resolved shear stress ratio concerning prismatic/pyramidal slip with respect to basal at room temperature.[5,42]

The presence of small equiaxed grains surrounding the elongated grains (Figure 5) indicates the occurrence of partial DRX even after room temperature deformation. However, the presence of high LAGB fraction in both the VR and FR cases (Figure 7) indicates a more deformed structure compared to the only ECAP-processed sample. A detailed analysis was carried out on the rolling plane ($^{\perp}$ND) of the VR sample, on which the basal planes are oriented (Figure 5). A high fraction of scattered 2 deg to 5 deg LAGBs and some 5 deg to 15 deg LAGBs was observed in the deformed grains (not shown for brevity). These grains can be seen to be surrounded by recrystallized grains that have orientations totally different from the deformed grains, as that occurs in DDRX. However, some of the grains do exhibit only a small deviation in orientation with respect to the deformed grains which are characteristics of CDRR.

The magnified EBSD map with superimposed unit cells of the TD section of the VR samples is shown in Figure 15. The grains are oriented in such a manner that the prismatic/pyramidal planes are nearly aligned parallel to the TD direction. It can be observed that the HCP unit cells of the recrystallized grains are at ~30 deg orientation relationship around the *c*-axis with respect to the deformed grains, thus indicating CDRR. At the same time, some of the recrystallized grains do not have any specific orientation relationship with the neighboring deformed grains indicating the occurrence of DDRX. Thus, similar to ECAP, both DRX mechanisms, CDRR and DDRX, are present at different locations and can be attributed to the relative influence of the type of slip system families; prismatic/pyramidal or basal, respectively. Ion *et al.*[45] have shown that insufficient number of slip systems at lower temperature in Mg alloys lead to local shearing and subsequent lattice rotation at the vicinity of grain boundaries to form new grains by CDRR. In the present study, a lesser extent of twinning (twin boundary fraction <1 pct) after

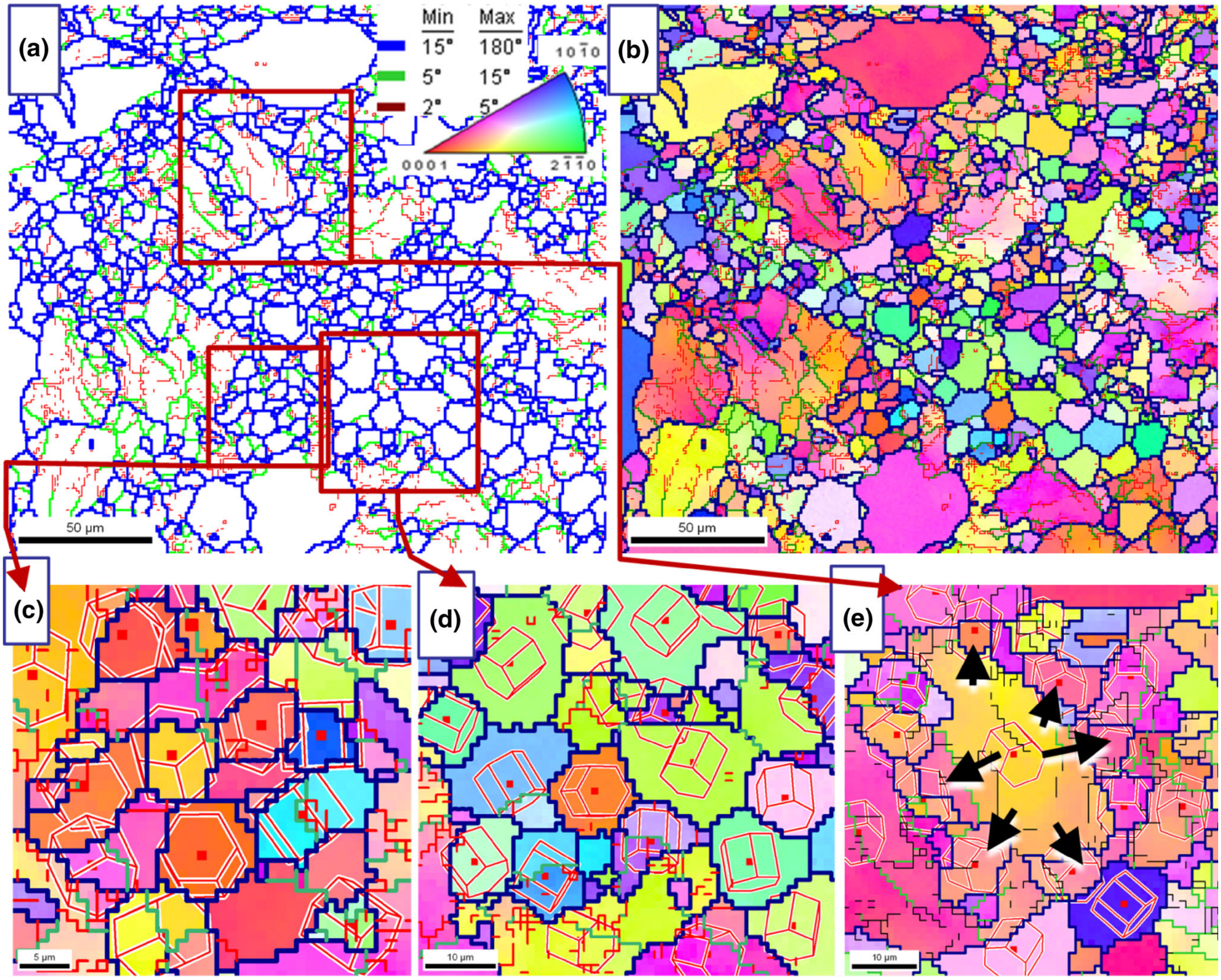

Fig. 14—Grain boundary map and magnified Inverse pole figure (IPF) maps with superimposed HCP unit cell as recorded on the 45 deg section of the Route A ECAP-processed pure Mg after four passes.

rolling indicates slip-dominated mechanism at room temperature.

B. *Effect of Static Recrystallization on the Microstructure*

1. *After ECAP only*

It is well known that DRX leads to remnant dislocation densities, and thus annealing will relax the microstructure by static recovery, recrystallization, and grain growth. In the case of ECAP by routes A and B_C, no noticeable grain growth occurred on annealing at 373 K (100 °C) for 1 hour. However, on annealing at 773 K (500 °C) grain growth was prevalent (Figures 2, 3). Moreover, for the route A condition, annealing at 373 K (100 °C) led to a decrease in LAGBs (Figure 4). The ECAP-processed microstructure, which was partially recovered and recrystallized, on annealing statically recovers by the transformation of very low-angle misorientations (<2 deg) to LAGBs and finally recrystallize from LAGB to HAGBs. On annealing at 773 K (500 °C), large grains form with low fraction of LAGB (Figures 2, 4). For route B_C, the LAGB fraction increases on annealing at 373 K (100 °C). This may be due to the rearrangement of the very low-angle misorientations (<2 deg) to form LAGBs and comparatively insignificant transformations of LAGB to HAGB. In this case, the predominance of recovery was observed. The increase in the LAGB fraction occurs even after annealing at 773 K (500 °C), Figure 4. A large fraction of annealing twins can be observed in this condition.

In order to analyze the SRX mechanism, magnified IPF maps with superimposed hexagonal unit cells are presented from the EBSD scans of the 373 K (100 °C) annealed sample for both ECAP conditions in Figure 16. The IPF maps in Figures 16(a) through (d) show that deformed grains are still present in the annealed micrographs. The arrows in the figure, starts from these deformed grains and ends on the recrystallized grains showing slight rotations of the unit cells around the basal axis. This clearly indicates that the mechanism is "continuous static recrystallization" (CSRX) corroborating the observations of Xu-Yue *et al.*[20] Tensile twins were also observed (circled in Figure 16(d)) in some parts of the microstructure.

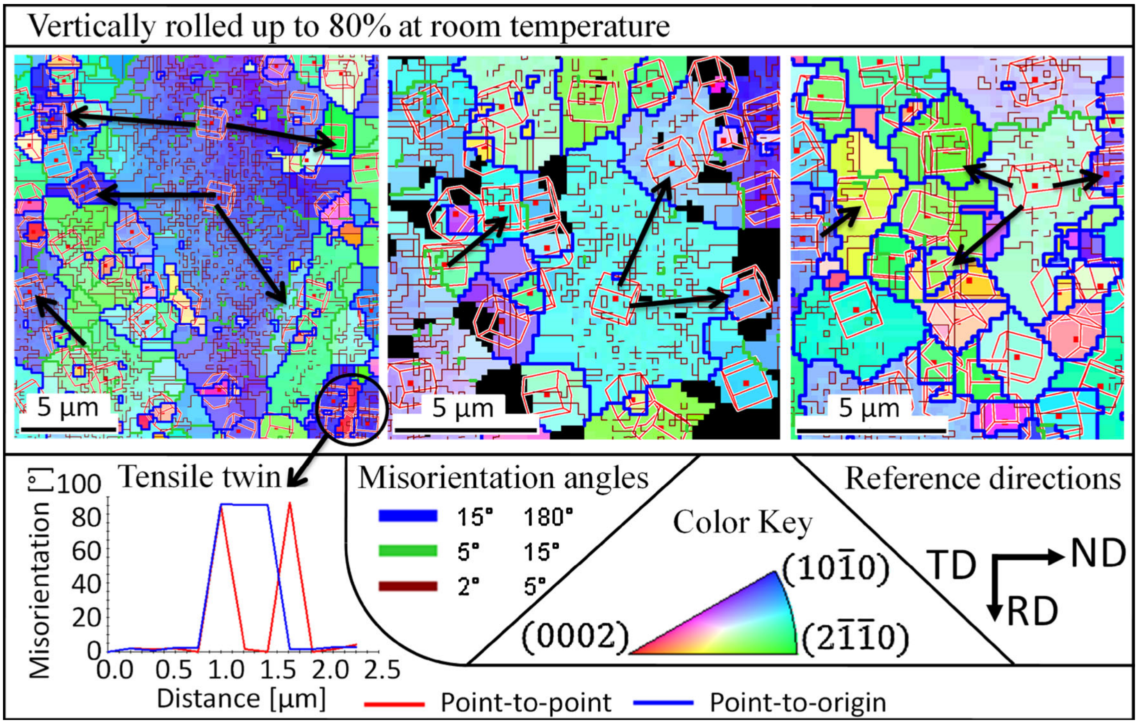

Fig. 15—Magnified Inverse pole figure (IPF) maps with superimposed HCP unit cell from different portions of the EBSD scans recorded on the TD plane of the 80 pct vertically rolled pure Mg.

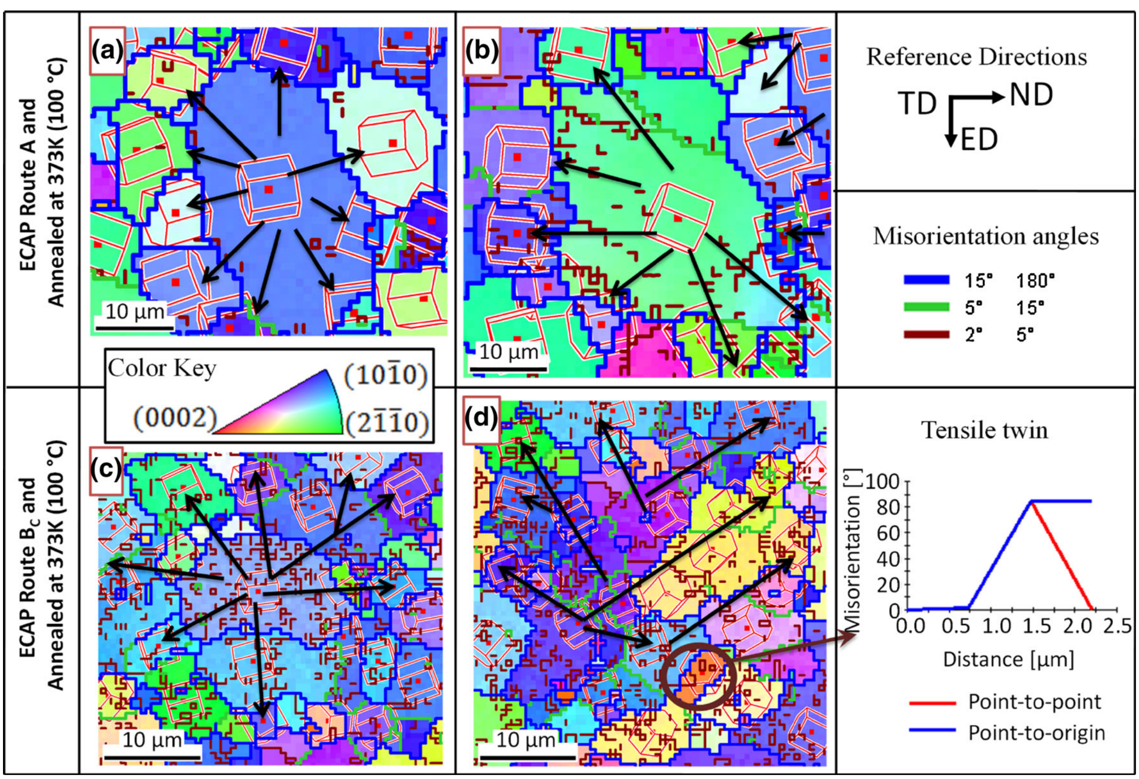

Fig. 16—Magnified Inverse pole figure (IPF) maps with superimposed HCP unit cell from different portions of the EBSD scans recorded on the TD plane of the Route A and B_C ECAP-processed and 373 K (100 °C) annealed pure Mg.

2. *ECAP + cold rolled*

Similar to the ECAP-processed Mg, annealing of the cold-rolled (VR and FR) Mg at 373 K (100 °C) led to small grain growth (Figures 5, 6). Massive grain growth took place on annealing at 773 K (500 °C) similar to the ECAP-processed samples. Interestingly, no decrease in the LAGB fraction could be observed on annealing at 373 K (100 °C) and at 773 K (500 °C) similar to the ECAP route B_C condition. It is well known that annealing consists of recovery, recrystallization, and grain growth. Recovery is the rearrangement of very low-angle misorientations (<2 deg) to form LAGB. In recrystallization, the LAGB increases their misorientation while migrating to form HAGB. Consecutively, grain growth occurs by the migration of HAGB by diffusion-related process to consume the comparatively more strained grains. As understood by the authors, the large LAGB fraction is due to the predominance of recovery over recrystallization. The large grain size after annealing at 773 K (500 °C) is the result of thermodynamic driving force gained by the reduction in the boundary area.

The SRX mechanism of the cold-rolled Mg can be observed in Figure 5 for the VR and FR, 373 K and 773 K (100 °C and 500 °C) annealed samples, respectively. Observation after annealing at 373 K (100 °C), Figure 5 (second column), shows that almost all recrystallized grains have basal orientation parallel to ND, the orientation relationship is ~30 deg rotation around the *c*-axis with respect to formerly deformed grains that are still present. This clearly indicates that static recovery and recrystallization, abbreviated as CSRX occurs suppressing the previously formed DDRX grains. It will be shown in Section IV–D–2 how these CSRX grains contribute to the changes in the texture. Figure 5 (third column) shows that after annealing at 773 K (500 °C) the previously formed DDRX grains disappear totally. The microstructure contains mostly large equiaxed grains. A large fraction of annealing twins can also be observed in the microstructure.

C. *Effect of Dynamic Recrystallization on Texture*

1. *ECAP*

The deformation texture after ECAP is usually attributed to simple shear at 45 deg to both ED and ND in a 90 deg die. Typical B and C_2 fibers form which are shifted due to the ECAP routes (A or B_C). The details of texture evolution and the description of fibers during ECAP of magnesium are given in references.[5,38] The effect of DRX on the deformation texture is very minimal and is not visible in the pole figures.[51] However, a faint distinction can be done from the $\varphi_2 = 0$ deg and 30 deg ODF sections (Figure 8). This is based on the criteria that in magnesium alloys, recrystallization leads to rotation of the recrystallized grains by 30 deg around $\langle 0002 \rangle$ axis from $\langle 2\bar{1}\bar{1}0 \rangle$ to $\langle 10\bar{1}0 \rangle$ with respect to the deformed grains.[39,44,52] It is well known that the deformation texture should have maximum intensity of the texture fiber in the $\varphi_2 = 0$ deg section. An equivalent or sometimes a little more intensity of the B and C_2 fibers in the $\varphi_2 = 30$ deg section is an indication of the presence of recrystallized grains. In the $\varphi = 90$ deg ODF section (Figure 9), the texture fibers are present from $\varphi_2 = 0$ deg to 60 deg, the maxima near to the $\varphi_2 \approx 30$ deg clearly indicate that the extent of DRX is very high during ECAP at 523 K (250 °C). However, the presence of unrecrystallized deformed grains cannot be ignored by the presence of the $\varphi_2 = 0$ deg to 60 deg texture fiber.

2. *Cold rolling*

Room temperature rolling was carried out up to 80 pct reduction in VR and FR configuration. A typical axisymmetric basal texture was formed along ND for both conditions irrespective of the initial textural differences (Figure 10). The effect of DRX on the texture is shown in the $\varphi = 90$ deg ODF section, Figure 12. In Figure 12(a), the presence of maxima in the $\varphi_2 =$ deg to 60 deg texture fiber at $\varphi_2 = 0$ deg and $\varphi_2 = 30$ deg for the VR configuration can be seen. Using the IQ criteria (Figure 11), the microstructure was partitioned as DRX and deformed grains. The $\varphi = 90$ deg ODF section of the DRX part shows the maximum texture intensity at $\varphi_2 = 30$ deg (Figure 12(b)), whereas the maximum texture intensity of the deformed part is at $\varphi_2 = 0$ deg (Figure 12(c)). A similar texture (as in Figure 12(a)) can be seen in the $\varphi = 90$ deg ODF section acquired from the EBSD scan of the TD surface for the VR Mg in Figure 12(d).

In Figure 12(i), the $\varphi = 90$ deg ODF section obtained from a viscoplastic self-consistent (VPSC) simulation for 80 pct rolling reduction is shown. It was found that the best agreement between experimental and simulation results for rolling at room temperature could be obtained using the following combination of the relative reference stresses: $[\tau_0^{\mathrm{basal}}/\tau_0^{\mathrm{prism}}/\tau_0^{\mathrm{pyr}\langle a\rangle}/\tau_0^{\mathrm{pyr}\langle c+a\rangle-\mathrm{I}}/\tau_0^{\mathrm{pyr}.\langle c+a\rangle-\mathrm{II}}]$: [1/8/8/6/6]. This CRSS ratio for different slip systems in Mg alloys was also used previously by different authors[38,49] and led to good agreements with experiments. It can be observed that the maximum intensity of the texture fiber is located at $\varphi_2 = 0$ deg and 60 deg left and right to the $\varphi_1 = 180$ deg orientation. These two fibers explain the wide experimental fibers (Figures 12(c) and (d)).

D. *Effect of Static Recrystallization on Texture*

1. *ECAP*

No change in the texture of the ECAP-processed samples could be observed on annealing at 373 K and 773 K (100 °C and 500 °C). However, the texture intensity of the fibers increased for both routes, see Figure 8. In the $\varphi = 90$ deg ODF section, the 30 deg rotation around $\langle 0002 \rangle$ due to SRX was also absent (Figure 9). As the ECAP was carried out at 523 K (250 °C), DRX took place during the severe plastic deformation leading to the formation of maxima at $\varphi_2 \approx 30$ deg on the $\varphi_2 = 0$ deg to 60 deg texture fiber. DRX during ECAP led to the modification of the texture to a recrystallized state. Thus, no changes, except intensification of the texture fibers could be observed on further recrystallization.

2. *Cold rolling*

Similar as in ECAP, no changes in the main components of the cold-rolled (VR and FR) texture can be detected on the pole figures and in the $\varphi_2 = 0$ deg and $\varphi_2 = 30$ deg ODF sections (Figure 10) of the 373 K and 773 K (100 °C and 500 °C) annealed conditions. However, the texture intensity increases with the annealing temperature. For the VR and FR samples annealed at 773 K (500 °C) for 1 hour, texture components at ~90 deg away from the rolling texture can be observed on both pole figures and in the $\varphi_2 = 0$ deg ODF section. These components are the consequence of the formation of tensile twins (Figure 7) during annealing (Figure 5). It has been shown earlier[23,24] that extensive annealing leads to abnormal grain growth, which renders the prismatic $\{11\bar{2}0\}$ planes parallel to the sheet plane.

In order to observe the effect of CSRX on the texture, the $\varphi = 90$ deg ODF section of the 373 K (100 °C) annealed conditions is plotted in Figure 12(e). A $\varphi_2 = 0$ deg to 60 deg texture fiber with maximum texture intensity at both $\varphi_2 = 0$ deg and 30 deg could be seen. Partitioning the microstructure using IQ shows that the CSRX part has a maximum texture intensity at $\varphi_2 = 30$ deg (Figure 12(f)), whereas the deformed part at $\varphi_2 = 0$ deg (Figure 12(g)). A high texture intensity at $\varphi_2 \approx 30$ deg could be observed for the sample annealed at [773 K (500 °C)] in Figure 12(h).

The shift in the texture components during DRX and SRX could be interpreted using the plastic power.[35,39] The plastic power is defined as $E(g) = \sum\sum \tau^{s,f}(g)\dot{\gamma}^{s,f}(g)$, where $\tau^{s,f}$ is the resolved shear stress in the slip system s of the family indexed by f and $\dot{\gamma}^{s,f}$ is the slip rate for a grain g. The map of plastic power was plotted for the $\varphi = 90$ deg ODF section on a grid of 1 deg using the VPSC approach for a small strain increment (0.01) in Figure 12(j). The DRX and SRX grains are expected to occur at locations in the ODF corresponding to the minimum plastic power. By comparing the plastic power map with the DRX and SRX ODFs in Figure 12, it can be verified that $\varphi_2 = 30$ deg position corresponds to a local minimum plastic power.

VI. CONCLUSIONS

The effect of dynamic, SRX, and grain growth on the deformation microstructure and texture of pure Magnesium was studied after Equal Channel Angular Pressing (ECAP by routes A and B_C) carried out at 773 K (500 °C) and after subsequent room temperature (vertical and flat) rolling (VR and FR) followed by annealing at 373 K and 773 K (100 °C and 500 °C) for 1 hour. The analyses of the results have led to the following main conclusions:

1. The microstructural features of the ECAP-processed and room temperature-rolled pure Mg indicate that the dynamic recrystallization mechanism is continuous dynamic recovery and recrystallization (CDRR) in regions where the prismatic/pyramidal slip activities are predominant and discontinuous dynamic recrystallization (DDRX) in other regions where the basal slip activity is higher. Anisotropy in the stacking fault energy, low for basal and high for prismatic/pyramidal planes could be responsible for such polymorphic behavior.
2. Continuous SRX was observed on annealing in both the ECAP and the room temperature-rolled magnesium. No significant grain growth occurred on annealing at 373 K (100 °C), but substantial grain growth took place on annealing at 773 K (500 °C).
3. A growth preference for 30 deg rotation around $\langle 0002\rangle$ axis from $\langle 2\bar{1}\bar{1}0\rangle$ to $\langle 10\bar{1}0\rangle$ of the recrystallized grains were observed with respect to the deformed grains during dynamic and SRX. The recrystallized grains form due to a rotation around their c-axis obeying the minimum plastic power criterion.
4. The formation of $\{10\bar{1}2\}$ tensile twins with orientation relationship of ~86 deg $\langle 11\bar{2}0\rangle$ was observed after annealing the room temperature-rolled pure magnesium at 773 K (500 °C). This leads to the formation of a texture component 86 deg away from the axisymmetric basal texture formed by rolling.

ACKNOWLEDGMENTS

This work was supported by the French State through the program "Investment in the future" operated by the National Research Agency (ANR) and referenced by ANR-11-LABX-0008-01 (LabEx DAMAS). The work also used the facility setup under the Institute Nanoscience Initiative sponsored by DST-FIST program at IISc, Bangalore. SB sincerely acknowledges the prolific discussions that took place with Profs. R. K. Ray, T. Watanabe, and J. A. Szpunar.

REFERENCES

1. A. Stalmann, W. Sebastian, H. Friedrich, S. Schumann, and K. Dröder: *Adv. Eng. Mater.*, 2001, vol. 3, pp. 969–74.
2. R. Reed-Hill and W. Robertson: *Trans. Met. Soc. AIME*, 1957, vol. 220, pp. 496–502.
3. J.W. Li, W. Xu, X.L. Wu, H. Ding, and K. Xia: *Mater. Sci. Eng. A*, 2011, vol. 528, pp. 5993–98.
4. S. Suwas, G. Gottstein, and R. Kumar: *Mater. Sci. Eng. A*, 2007, vol. 471, pp. 1–14.
5. S. Biswas, D.S. Singh, and S. Suwas: *Acta Mater.*, 2010, vol. 58, pp. 3247–61.
6. M. Mabuchi, K. Ymeyama, H. Iwasaki, and K. Higashi: *Acta Mater.*, 1999, vol. 47, pp. 2047–57.
7. S. Kamodo, T. Ashie, H. Yamada, K. Sanbun, and Y. Kojima: *Mater. Sci. Forum*, 2000, vol. 65, pp. 350–51.
8. S.R. Agnew, G.M. Stoica, L. Chen, T.M. Lillo, J. Macheset, and P.K. Liaw: in *Ultra Fine Grain Materials II*, Y.T. Zhu, T.G. Langdon, R.S. Mishra, S.L. Semiatin, M.J. Saran, and T.C. Lowe, eds., TMS, Warrendale, PA, 2002, pp. 643–652.
9. J. Koike, T. Koboyashi, T. Mukai, H. Watanabe, M. Suzuki, K. Muruyama, and K. Higashi: *Acta Mater.*, 2003, vol. 51, pp. 2055–65.
10. M.R. Barnett, Z. Keshavarz, A.G. Beer, and D. Atwell: *Acta Mater.*, 2004, vol. 52, pp. 5093–03.
11. T. Mukai, M. Yananoi, H. Watanabe, and K. Higashi: *Scripta Mater.*, 2001, vol. 45, pp. 89–94.
12. W.J. Kim, C.W. An, Y.S. Kim, and S.I. Hong: *Scripta Mater.*, 2002, vol. 47, pp. 39–44.
13. T. Mukai, Y. Masashi, and K. Iligashi: *Mater. Trans., JIM*, 2001, vol. 42, pp. 2652–54.
14. R. Gehrman and G. Gottstein: in *Proc. of ICOTOM-12*, J. A. Szpuner, ed., NRC Research Press, Montreal, vol. 1, 1999, pp. 665–70.
15. H.Y. Chao, H.F. Sun, W.Z. Chen, and E.D. Wang: *Mater. Charact.*, 2011, vol. 62, pp. 312–20.
16. A. Jäger, P. Lukac, V. Gartnerova, J. Haloda, and M. Dopita: *Mater. Sci. Eng. A*, 2006, vol. 432, pp. 20–25.

17. K. Hantzsche, J. Bohlen, J. Wendt, K.U. Kainer, S.B. Yi, and D. Letzig: *Scripta Mater*., 2010, vol. 63, pp. 725–30.
18. É. Martin and J.J. Jonas: *Acta Mater*., 2010, vol. 58, pp. 4253–66.
19. Z. Zhang, M.-P. Wang, N. Jiang, and S.-M. Li: *Mater. Sci. Eng. A*, 2010, vol. 527, pp. 6467–73.
20. Y. Xu-Yue, H. Himura, and T. Sakai: *Trans. Nonfer. Met. Soc. China*, 2007, vol. 17, pp. 1139–42.
21. A. Yamamoto, M. Kakishiro, M. Ikeda, and H. Tsubakino: *Mat. Sc. Forum*, 2004, vols. 449–452, pp. 669–73.
22. S.W. Su, L. Lu, and M.O. Lai: *Phil. Mag*., 2008, vol. 88, pp. 181–200.
23. M.T. Pérez-Prado and O.A. Ruano: *Scripta Mater*., 2002, vol. 46, pp. 149–55.
24. M.T. Pérez-Prado and O.A. Ruano: *Scripta Mater*., 2003, vol. 48, pp. 59–64.
25. X.Y. Yang, H. Miura, and T. Sakai: *Mater. Trans*., 2005, vol. 46, pp. 2981–87.
26. L.W.F. Mackenzie and M. Pekguleryuz: *Mater. Sci. Eng. A*, 2008, vol. 480, pp. 189–97.
27. S. Abdessameud and D. Bradai: *Can. Metall. Q*., 2009, vol. 48, pp. 433–42.
28. X. Huang, K. Suzuki, and Y. Chino: *Mater. Sc. Eng. A*, 2013, vol. 560, pp. 232–40.
29. É. Martin, L. Jiang, S. Godet, and J.J. Jonas: *Int. J. Mater. Res*., 2009, vol. 100, pp. 576–83.
30. S.B. Yi, I. Schestakow, and S. Zaefferer: *Mater. Sci. Eng., A*, 2009, vol. 516, pp. 58–64.
31. K. Hantzsche, J. Bohlen, J. Wendt, K.U. Kainer, S.B. Yi, and D. Letzig: *Scripta Mater*., 2010, vol. 63, pp. 725–30.
32. L. Lu, T. Liu, M-J Tan, J. Chen, and Z. Wang: *Mater. Des*., 2012, vol. 39, pp. 131–39.
33. A. Ostapovets, P. Šedá, A. Jäger, and P. Lejček: *Scripta Mater*., 2011, vol. 64, pp. 470–73.
34. J.P. Mathieu, S. Suwas, A. Eberhardt, L.S. Toth, and P. Moll: *J. Mater. Proc. Technol*., 2006, vol. 173, pp. 29–33.
35. S. Biswas, B. Beausir, L.S. Toth, and S. Suwas: *Acta Mater*., 2013, vol. 61, pp. 5263–77.
36. L.S. Toth, S. Biswas, B. Beausir, and C.-F. Gu: *Mater Charact*., 2013, vol. 84, pp. 67–71.
37. B. Beausir, L.S. Toth, and K.W. Neale: *Acta Mater*., 2007, vol. 55, pp. 2695–05.
38. B. Beausir, S. Suwas, L.S. Toth, K.W. Neale, and J.J. Fundenberger: *Acta Mater*., 2008, vol. 56, pp. 200–214.
39. B. Beausir, S. Biswas, D.-I. Kim, L.S. Toth, and S. Suwas: *Acta. Mater*., 2009, vol. 57, pp. 5061–77.
40. Y. Zhong, F. Yin, T. Sakaguchi, K. Nagai, and K. Yang: *Acta Mater*., 2007, vol. 55, pp. 2747–56.
41. S. Biswas, D.S. Singh, A. Bhowmik, and S. Suwas: *Mater. Sci. Forum*, 2008, vols. 584–586, pp. 343–84.
42. A.E. Smith: *Surf. Sci*., 2007, vol. 601, pp. 5762–65.
43. L. Jin, D. Lin, D. Mao, X. Zeng, B. Chen, and W. Ding: *Mater. Sci. Eng. A*, 2006, vol. 423, pp. 247–52.
44. R.K. Nadella, I. Samajdar, and G. Gottstein: in *Proc. Magnesium Alloys and their Applications*, K.U. Kainer ed., Wiley-VCH, Weinheim 2003, p. 1052.
45. S.E. Ion, F.J. Humphreys, and S.H. White: *Acta. Metal*., 1982, vol. 30, pp. 1909–19.
46. F.J. Humphreys and M. Hatherly: *Recrystallization and Related Annealing Phenomena*, 2nd ed., Elsevier, Oxford, 2004.
47. A. Galiyev, R. Kaibyshev, and G. Gottstein: *Acta Mater*., 2001, vol. 49, pp. 1199–1207.
48. J.C. Tan and M.Y. Tan: *Mater. Sci. Eng. A*, 2003, vol. 339, pp. 124–32.
49. S.R. Agnew, P. Mehrotra, T.M. Lillo, G.M. Stoica, and P.K. Liaw: *Mater. Sci. Eng. A*, 2005, vol. 408, pp. 72–78.
50. X. Shen, L. Lian, Z. Jiang, and Q. Jiang: *Mater. Sci. Eng. A*, 2008, vol. 487, pp. 410–16.
51. J.A. del Valle and O.A. Ruano: *Mater. Sci. Eng. A*, 2008, vol. 487, pp. 473–80.
52. S. Biswas, D.-I. Kim, and S. Suwas: *Mater. Sci. Eng. A*, 2012, vol. 550, pp. 19–30.